Superconducting properties of La$_2$(Cu$_{1-x}$Ni$_x$)$_5$As$_3$O$_2$: A μSR study

Qiong Wu [1], Kaiwen Chen [1], Zihao Zhu,[1] Cheng Tan,[1] Yanxing Yang,[1] Xin Li [1], Toni Shiroka [2,3] Xu Chen [4] Jiangang Guo,[4] Xiaolong Chen,[4] and Lei Shu [1,5,6,*]

[1]*State Key Laboratory of Surface Physics, Department of Physics, Fudan University, Shanghai 200438, People's Republic of China*
[2]*Laboratory for Muon-Spin Spectroscopy, Paul Scherrer Institute, CH-5232 Villigen PSI, Switzerland*
[3]*Laboratorium für Festkörperphysik, ETH Zürich, CH-8093 Zürich, Switzerland*
[4]*Beijing National Laboratory for Condensed Matter Physics, Institute of Physics, Chinese Academy of Sciences,*
P.O. Box 603, Beijing 100190, China
[5]*Collaborative Innovation Center of Advanced Microstructures, Nanjing 210093, People's Republic of China*
[6]*Shanghai Research Center for Quantum Sciences, Shanghai 201315, People's Republic of China*

We report the results of muon spin rotation and relaxation (μSR) measurements on the recently discovered layered Cu-based superconducting material La$_2$(Cu$_{1-x}$Ni$_x$)$_5$As$_3$O$_2$ ($x = 0.40$ and 0.45). Transverse-field μSR experiments on both samples show that the temperature dependence of superfluid density is best described by a two-band model. The absolute values of zero-temperature magnetic penetration depth $\lambda_{ab}(0)$ were found to be 427(1.7) and 422(1.5) nm for $x = 0.40$ and 0.45, respectively. Both compounds are located between the unconventional and the standard BCS superconductors in the Uemura plot. No evidence of time-reversal symmetry breaking in the superconducting state is suggested by zero-field μSR measurements.

I. INTRODUCTION

The relation between magnetism and superconductivity is one of the most prominent issues in condensed matter physics [1–10]. Since the discovery of cuprate high transition temperature (T_c) superconductors, considerable efforts have been made to investigate the role of in-plane impurities in them. It is now well established that, in copper oxide superconductors, nonmagnetic Zn ions suppress T_c even more strongly than magnetic Ni ions [11–14]. Such behavior is in sharp contrast to that of conventional BCS superconductors, in which magnetic impurities can act as pair-breaking agents, rapidly suppressing superconductivity [15,16]. Another interesting behavior of unconventional superconducting systems such as the heavy-fermion, high T_c cuprate, and iron-pnictide superconductors is the dome shape of the chemical doping dependence of T_c [17–20].

Recently, the first Cu-As superconductor was discovered in layered La$_2$Cu$_5$As$_3$O$_2$ with $T_c = 0.63$ K [21]. When Cu^{2+} is replaced by Ni^{2+}, also in La$_2$(Cu$_{1-x}$Ni$_x$)$_5$As$_3$O$_2$, the T_c exhibits a domelike structure. Remarkably, while the superconductivity in cuprate- and iron-based superconductors is completely suppressed when the substitution ratio of Cu or Fe exceeds 20% [22,23], superconductivity in La$_2$(Cu$_{1-x}$Ni$_x$)$_5$As$_3$O$_2$ persists until the substitution ratio exceeds 60% [21]. In this case, the robustness of superconductivity reveals the unexpected effect of impurities on inducing and enhancing superconductivity. Hence, La$_2$(Cu$_{1-x}$Ni$_x$)$_5$As$_3$O$_2$ provides a broader platform for studying the doping effect in the superconducting phase diagram.

Specific heat measurements have revealed that the optimally doped La$_2$(Cu$_{1-x}$Ni$_x$)$_5$As$_3$O$_2$ ($x = 0.40$) sample shows a sharp superconducting transition at $T_c = 2.05$ K, with a dimensionless jump $C_e/\gamma_s T_c = 1.42$ [21], consistent with the BCS weak-coupling limit (1.43). In the superconducting state, the temperature dependence of the specific heat coefficient is described by a fully gapped model $C_e/T \propto e^{-\Delta/k_B T}$ after subtracting the upturn of C_e/T below $T < 0.5$ K, which is attributed to the Schottky effect. These results suggest that La$_2$(Cu$_{1-x}$Ni$_x$)$_5$As$_3$O$_2$ ($x = 0.40$) is a conventional BCS superconductor with a fully developed energy gap. However, the fit yields $2\Delta/k_B T_c = 2.58$ [21], much smaller than the BCS weak-coupling limit.

Muon spin rotation and relaxation (μSR) experiments have been widely utilized to probe superconductivity in type-II superconductors at the microscopic level [24], and they are free from the influence of the Schottky effect. Transverse-field (TF) μSR measures the absolute value of the magnetic penetration depth λ, which is related to the density of superconducting carriers. The temperature dependence of λ is sensitive to the lowest-lying superconducting excitations and provides information on the symmetry of superconducting pairing [25–30]. In addition, zero-field (ZF) μSR is a powerful method to detect small spontaneous internal magnetic fields due to the possible breaking of time-reversal symmetry (TRS) at the superconducting transition. These can be as small as 10 μT, corresponding to about 10^{-2} of Bohr magneton μ_B [24,25,31–34].

Here, in order to study the doping effect on superconductivity, we perform μSR measurements on polycrystalline samples of La$_2$(Cu$_{1-x}$Ni$_x$)$_5$As$_3$O$_2$ for $x = 0.40$ (optimal doping) and $x = 0.45$ (overdoped). The temperature dependence of superfluid density determined from TF-μSR is best

---

*Corresponding author: leishu@fudan.edu.cn

described by a two-band superconductivity model. d-wave superconductivity possibly exists in one of the bands, with a fraction of the d wave smaller in the overdoped sample than that in the optimally doped one. The superconducting energy gap is larger for optimal doping, suggesting that the coupling strength decreases with an increase of doping. Both compounds are located between the unconventional and the standard BCS superconductors in the Uemura plot. Meanwhile, no evidence of TRS breaking is suggested by ZF-μSR measurements.

II. EXPERIMENTAL DETAILS

Solid-state reactions were used to produce polycrystalline samples of La$_2$(Cu$_{1-x}$Ni$_x$)$_5$As$_3$O$_2$ ($x = 0.40$ and 0.45) [21]. The performed x-ray diffraction (XRD) studies and the density functional theory (DFT) calculation shows the band structures of La$_2$Cu$_5$As$_3$O$_2$, indicating that this newly synthesized sample is a layered superconducting compound, with superconducting atomic layers consisting of a [Cu$_5$As$_3$]$^{2-}$ cagelike structure [21].

μSR experiments were carried out using nearly 100% spin-polarized positive muons (μ^+) on the M15 beamline at TRIUMF, Vancouver, Canada for $x = 0.40$, and the DOLLY spectrometer of the SμS muon source at Paul Scherrer Institute (PSI), Switzerland for $x = 0.45$, respectively. The samples were mounted on a silver sample holder at TRIUMF and a copper sample holder at PSI, respectively. Only a very limited amount of muons stopped in the extremely thin copper sample holder. In TF-μSR measurements, where the external field is applied perpendicular to the initial muon spin polarization, muons are implanted one at a time into a sample which is cooled (from above T_c) in an external magnetic field. Muon spins precess around the local field at the implantation site, and the functional form of the muon spin polarization depends on the field distribution of the vortex state, including the magnetic penetration depth, the vortex core radius, and the structure of the flux-line lattice. For ZF-μSR measurements, the ambient magnetic field was actively compensated to better than 1 µT. μSR data were analyzed using the MUSRFIT software package [35].

III. RESULTS

A. Transverse-field μSR experiments

The μSR asymmetry spectrum usually consists of a signal from muons that stop in the sample and a slowly relaxing background signal from muons that miss the sample, for example, stop in the sample holder. Figures 1(a) and 1(b) show the typical TF-μSR muon spin precession signals at an applied field of $\mu_0H = 30$ mT in the normal (red squares) and superconducting states (blue circles) for La$_2$(Cu$_{1-x}$Ni$_x$)$_5$As$_3$O$_2$ ($x = 0.40$ and 0.45) after subtracting the background signal. The superconducting volume fractions are estimated to be 60% and 70% from the TF-μSR asymmetry at long times for $x = 0.40$ and 0.45, respectively. Figures 1(c) and 1(d) show the Fourier transformations (FFTs) of the total TF-μSR asymmetry. It can be inferred from the figure that vortex states are constructed in both samples at low temperatures [36]. Figures 1(e) and 1(f) show the details of
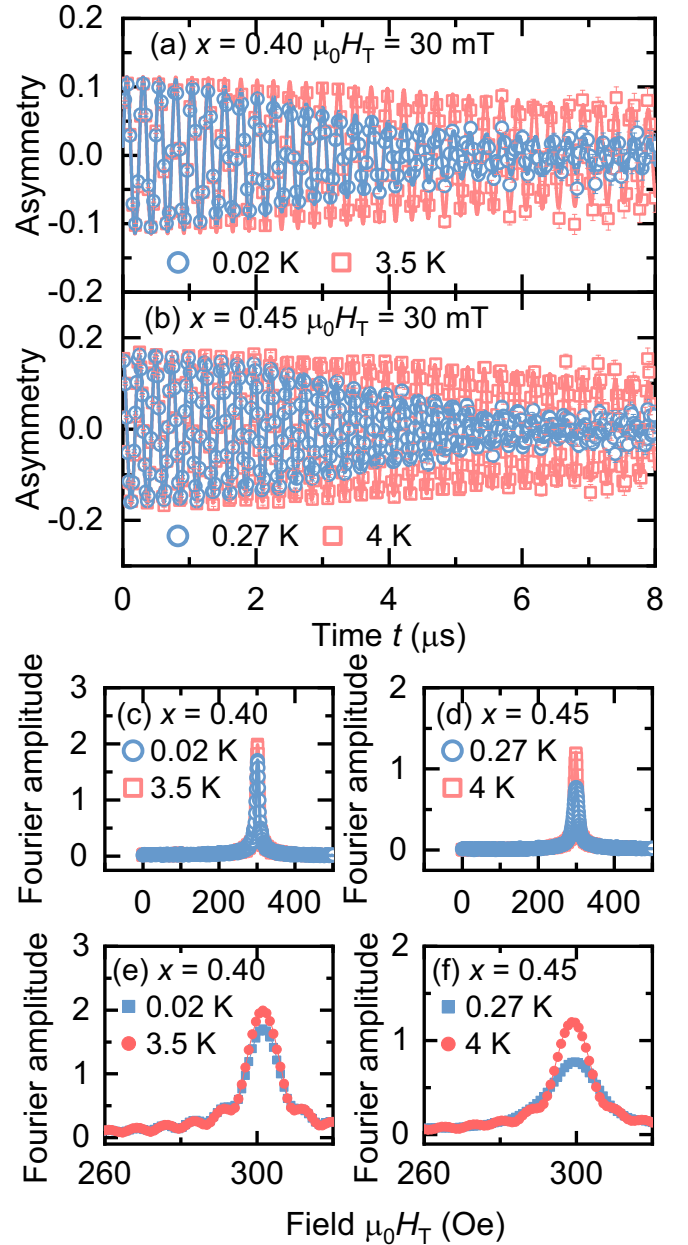

FIG. 1. (a), (b) Representative TF-μSR asymmetry spectra $A(t)$ for La$_2$(Cu$_{1-x}$Ni$_x$)$_5$As$_3$O$_2$ [(a) $x = 0.40$ and (b) 0.45] in the normal (red squares) and superconducting (blue circles) states with an external magnetic field of $\mu_0H = 30$ mT after subtracting the background signal. Solid curves: Fits to the data using Eq. (1). (c)–(f) Fourier transformation of the total TF-μSR time spectra. (e) and (f) show the details of the FFT spectra.

the FFT spectra. As shown in the figure, the magnetic fields in the superconducting state and the normal state are relatively close to each other. This is common in anisotropic powder superconducting samples [37,38].

The TF-μSR time spectra after subtracting the background signal can be well fitted by the function

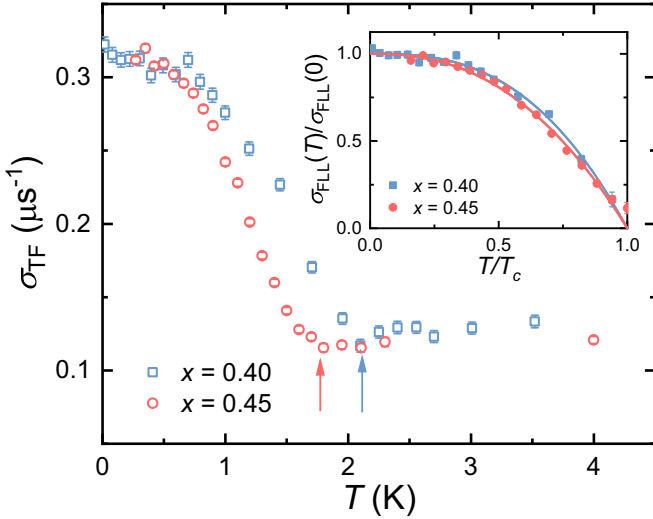$$A(t) = A_0 \exp\left(-\tfrac{1}{2}\sigma_{TF}^2 t^2\right)\cos(\gamma_\mu B_s t + \varphi_s), \quad (1)$$

FIG. 2. Temperature dependencies of the TF-μSR Gaussian relaxation rate σ_{TF} in La$_2$(Cu$_{1-x}$Ni$_x$)$_5$As$_3$O$_2$ ($x = 0.40$ and 0.45) for $\mu_0 H = 30$ mT. The arrows indicate T_c from resistivity measurements [21]. Inset: The normalized superfluid density $\sigma_{FLL}(T)/\sigma_{FLL}(0)$ from Eq. (2) vs the reduced temperature T/T_c. Solid curves: Phenomenological two-fluid model fits (see text).

where A_0 is the initial asymmetry of the muon spin in the sample. The Gaussian relaxation rate σ_{TF} due to the nuclear dipolar fields in the normal state is enhanced in the superconducting state due to the field broadening generated by the emergence of the flux-line lattice (FLL). $\gamma_\mu = 8.516 \times 10^8$ s^{-1} T^{-1} is the gyromagnetic ratio of the muon, and B_s is the magnetic field at muon stopping sites.

Figure 2 shows the temperature dependence of σ_{TF} obtained from the fits using Eq. (1) for La$_2$(Cu$_{1-x}$Ni$_x$)$_5$As$_3$O$_2$ ($x = 0.40$ and 0.45). There are noticeable upturns in σ_{TF} that develop below $T_c = 2.2$ and 1.8 K, respectively. The internal field distribution in the vortex state is the convolution of the FLL field distribution and the nuclear dipolar field distribution of the host material:

$$\sigma_{TF} = \begin{cases} \sqrt{\sigma_{FLL}^2 + \sigma_{dip}^2} & (T \leqslant T_c), \\ \sigma_{dip} & (T > T_c). \end{cases} \quad (2)$$

Above T_c, $\sigma_{TF} = \sigma_{dip}$ generated from the nuclear dipolar fields is roughly independent of temperature. Therefore, it was fixed to the average value [0.1179(11) μs^{-1} for $x = 0.45$ and 0.127(2) μs^{-1} for $x = 0.40$]. The value of σ_{dip} is smaller for larger x, consistent with the fact that the nuclear magnetic moment of nickel is smaller than that of copper [39].

In the inset of Fig. 2, the normalized FLL relaxation rate $\sigma_{FLL}(T)/\sigma_{FLL}(0)$ is plotted versus the reduced temperature T/T_c for $x = 0.40$ and 0.45. The data can be fitted with the phenomenological two-fluid model [40,41]

$$\sigma_{FLL}(T) = \sigma_{FLL}(0)[1 - (T/T_c)^N] \quad (T \leqslant T_c). \quad (3)$$

The fitting parameters are listed in Table I. There are several common predictions for the value of N. For traditional BCS superconductors, $N \sim 4$. However, both values of N for $x = 0.40$ and 0.45 are much lower than 4. The dirty-limit d-wave model predicts a value of $N = 2$ [42,43].

TABLE I. Parameters from fits to TF-μSR data using the phenomenological two-fluid model for La$_2$(Cu$_{1-x}$Ni$_x$)$_5$As$_3$O$_2$.

Parameters	$x = 0.40$	$x = 0.45$
$\sigma_{FLL}(0)$ (μs^{-1})	0.287(2)	0.300(4)
T_c (K)	2.08(4)	1.70(2)
N	2.72(17)	2.38(13)
$\lambda_{eff}(0)$ (nm)	559.4(1.9)	547(3)
$\lambda_{ab}(0)$ (nm)	427.02(1.49)	418(3)
σ_{dip} (μs^{-1})	0.127(2)	0.1179(11)
Adj. R^2	0.98443	0.99172

However, in the La$_2$(Cu$_{1-x}$Ni$_x$)$_5$As$_3$O$_2$ system, the upper critical field $H_{c2}(0)$ is estimated to be 3 T [21], giving an estimated value of the Ginzburg-Landau coherence length $\xi(0) = [\Phi_0/2\pi H_{c2}(0)]^{1/2} = 10.47$ nm, where $\Phi_0 = 2.07 \times 10^{-3}$ T m^2 represents the magnetic flux quantum. Given the metallic behavior, the mean free path can be estimated by $l_e = \hbar k_F/\rho_0 n e^2$ [44], with residual resistivity $\rho_0 = 0.34$ mΩ cm [21], yielding $l_e = 15$ nm for $x = 0.40$. Thus, La$_2$(Cu$_{1-x}$Ni$_x$)$_5$As$_3$O$_2$ may be a relatively clean superconductor with $\xi/l_e \approx 1$. The predicted clean-limit d-wave model N value is $N = 1$ [45]. As a result, our system may include both s and d waves.

For powder superconductor samples with $0.13/\kappa^2 \ll H/H_{c2} \ll 1$ ($\kappa = \lambda/\xi$ is the Ginzburg-Laudau parameter, and H is the applied field), the Gaussian depolarization rate σ_{FLL} is directly related to the magnetic penetration depth λ_{eff} by [46,47]

$$\frac{\sigma_{FLL}}{\gamma_\mu} = \frac{0.172(1-b)[1 + 1.21(1 - \sqrt{b})^3]\Phi_0}{2\pi\lambda_{eff}^2}, \quad (4)$$

where b is the reduced applied field $b = H/H_{c2} = 0.01 \ll 1$. Therefore, the absolute values of effective magnetic penetration depth $\lambda_{eff}(0)$ can be obtained and listed in Table I. In addition, for layered superconductors, the in-plane magnetic penetration depth $\lambda_{ab}(0)$ is also estimated by the relation $\lambda_{eff}(0) = 3^{1/4}\lambda_{ab}(0)$ [27,48,49].

The effective magnetic penetration depth λ_{eff} for isotropic superconductors is related to the density n_s of superconducting carriers and m^* by the general London equation [40]

$$\lambda_{eff}^2 = \frac{m^*}{\mu_0 e^2 n_s}, \quad (5)$$

where μ_0 is the magnetic constant, m^* is the effective electron mass, and e is the elementary charge. Therefore, the FLL relaxation rate σ_{FLL} is directly related to the superfluid density through $\sigma_{FLL} \propto \lambda_{eff}^{-2} \propto n_s$. Then we can use microscopic models to investigate the gap symmetry of La$_2$(Cu$_{1-x}$Ni$_x$)$_5$As$_3$O$_2$ in more detail, as shown in Fig. 3.

The single-gap model is defined within the local London approximation [50]

$$\frac{\sigma_{FLL}(T)}{\sigma_{FLL}(0)} = 1 + \frac{1}{\pi} \int_0^{2\pi} \int_{\Delta(T,\varphi)}^{\infty} \frac{\partial f(E)}{\partial E} \frac{E \, dE \, d\varphi}{\sqrt{E^2 - \Delta^2(T,\varphi)}}, \quad (6)$$

$$\Delta(T,\varphi) = \Delta_0 \delta(T/T_c) g(\varphi), \quad (7)$$

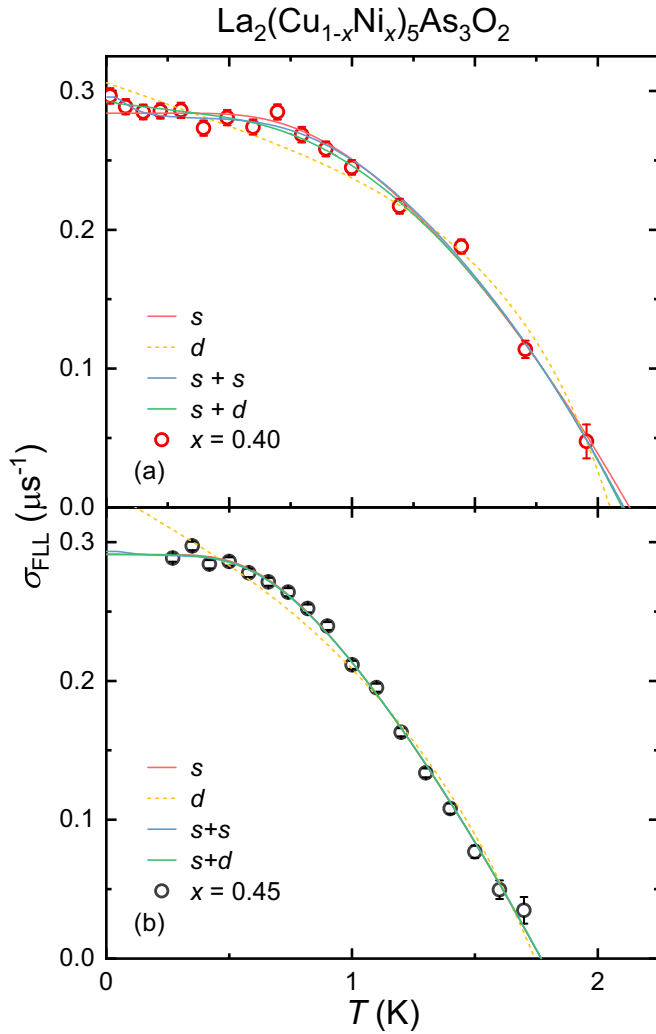$$\delta(T/T_c) = \tanh\{1.82[1.018(T_c/T - 1)]^{0.51}\}, \quad (8)$$

FIG. 3. The FLL relaxation rate $\sigma_{\mathrm{FLL}}(T)$ from Eq. (2) vs temperature for La$_2$(Cu$_{1-x}$Ni$_x$)$_5$As$_3$O$_2$: (a) $x = 0.40$ and (b) 0.45. Curves correspond to the s-wave, d-wave, $s + s$-wave, and $s + d$-wave models.

where $\sigma_{\mathrm{FLL}}(0)$ is the FLL relaxation rate at zero temperature, $f(E)$ is the Fermi-Dirac distribution function, φ is the angle along the Fermi surface, and Δ_0 is the maximum superconducting gap value at $T = 0$. $g(\varphi)$ in Eq. (7) describes the

angular dependence of the superconducting gap. Here, $g(\varphi) = 1$ and $|\cos(2\varphi)|$ refers to the s-wave and d-wave model, respectively.

The fitting parameters are listed in Table II. It is clear from Fig. 3 that the d-wave model (the dashed yellow lines) does not fit the data, also evidenced by the largest χ^2_{red} in Table II. The solid red curves in Fig. 3 representing the s-wave model seem to fit the data well giving the reduced chi-square $\chi^2_{\mathrm{red}} = 1.74$ and 2.19 for $x = 0.40$ and 0.45, respectively. Thus our results preliminarily suggest the s-wave pairing for both overdoped and underdoped samples for La$_2$(Cu$_{1-x}$Ni$_x$)$_5$As$_3$O$_2$ ($x = 0.45$ and 0.40). $\Delta(0)$ is larger for the optimal doping sample, suggesting the coupling strength decreases with the increase of doping concentration.

However, we notice that the superfluid density of $x = 0.40$ has a minor upturn at low temperatures. This may be due to nodal or multiband superconductivity. As a result, in addition to single-gap functions, we also employ the phenomenological two-gap α model with a weighting factor f_{Δ_1} [51–53],

$$\frac{\sigma_{\mathrm{FLL}}(T)}{\sigma_{\mathrm{FLL}}(0)} = f_{\Delta_1} \frac{\sigma_{\mathrm{FLL},\Delta_1}(T)}{\sigma_{\mathrm{FLL},\Delta_1}(0)} + (1 - f_{\Delta_1}) \frac{\sigma_{\mathrm{FLL},\Delta_2}(T)}{\sigma_{\mathrm{FLL},\Delta_2}(0)}, \quad (9)$$

where $\sigma^{-2}_{\mathrm{FLL},\Delta_i}(T)/\sigma^{-2}_{\mathrm{FLL},\Delta_i}(0)$ ($i = 1, 2$) is the superfluid density contribution of one of the gaps.

While the smallest χ^2_{red} in both compounds suggests that the $s + s$ model may be the best model, the resulting values of $2\Delta_2/k_BT_c$ are unreasonably small. The $s + d$ model is also better than the s-wave model according to the χ^2_{red} values. Moreover, the gap-to-T_c ratios $2\Delta_{1,2}/k_BT_c$ determined from the $s + d$ model are also close to the BCS theoretical predictions [$2\Delta_s/k_BT_c = 3.43(3)$ for s wave, and $2\Delta_d/k_BT_c = 4.15(3)$ for d wave, respectively) for $x = 0.45$. Both $s + s$ and $s + d$ models can well deal with the upwarping phenomenon of superfluid density at low temperatures in $x = 0.40$. However, we also notice that the relaxation rate of $x = 0.45$ does not show obvious upwarping at the current lowest temperature of 0.27 K, and also the obtained f_{Δ_d} values for both compounds are extremely small. More studies are needed to determine whether d-wave superconductivity exists in one of the bands.

B. Uemura plot

An Uemura plot [54–56] is shown in Fig. 4, including elemental superconductors (such as Nb, Al, Sn, and

TABLE II. Parameters from the fits to the single-gap and two-gap models from TF-μSR data. The weighting factor of phenomenological two-gap α model f_{Δ_1}, zero-temperature superconducting gap $\Delta(0)$, zero-temperature magnetic penetration depth $\lambda_{ab}(0)$, and reduced χ^2_{red} from fits of Eqs. (6) and (9).

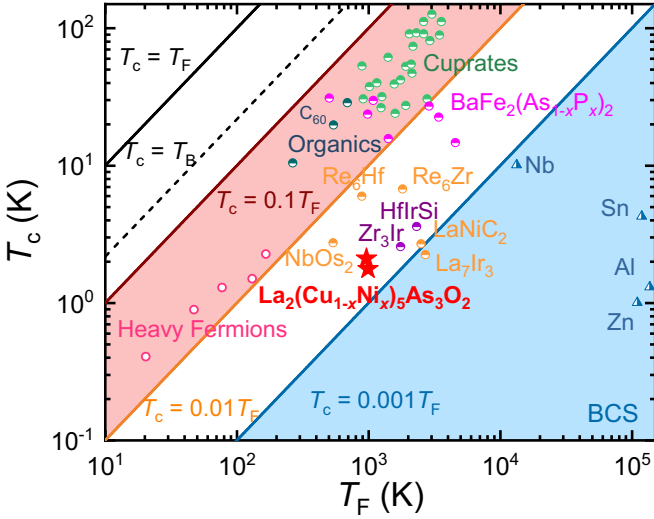| Ni doping	Model	f_{Δ_1}	$2\Delta_1/k_BT_c$	$2\Delta_2/k_BT_c$	$\lambda_{ab}(0)$ (nm)	χ^2_{red}
0.40	s	1	3.69(17)		427.4(1.8)	1.74
	d	1	6.68(37)		411(3)	4.46
	$s + s$	0.95(3)	3.86(17)	0.20(13)	419(5)	1.31
	$s + d$	0.70(12)	4.03(21)	5.62(7)	422(3)	1.50
0.45	s	1	3.34(7)		421.5(1.7)	2.19
	d	1	5.09(26)		392(5)	12.9
	$s + s$	0.988(154)	3.42(2)	0.262(2)	420(31)	2.06
	$s + d$	0.976(114)	3.43(3)	4.15(3)	422(5)	2.09

FIG. 4. The Uemura classification scheme [54,55,57]. The superconducting transition temperature T_c vs the effective Fermi temperature T_F, where the position of $La_2(Cu_{1-x}Ni_x)_5As_3O_2$ ($x = 0.45$ and 0.40) is shown by the red stars. The unconventional superconductors fall within a band indicated by the red and orange lines. The BCS superconductors are in the lower right region with blue marks.

Zn), cuprates, alkali-doped C_{60} (K_3C_{60} and Rb_3C_{60}), heavy-fermion superconductors, and $La_2(Cu_{1-x}Ni_x)_5As_3O_2$. In this classification, unconventional superconductors usually lie in the orange area for $1/100 \leqslant T_c/T_F \leqslant 1/10$, and conventional BCS superconductors fall in the blue region for $T_c/T_F \leqslant 1/1000$, where T_F is the Fermi temperature [40,55].

For the quasi-two-dimensional (2D) systems, T_F can be estimated by the following relation [40,58],

$$k_B T_F = \frac{\pi \hbar^2 n_{2D}^s}{m^*}, \qquad (10)$$

where n_{2D}^s is the two-dimensional superfluid density within the superconducting planes derived from the in-plane superfluid density via $n_{2D}^s = n_{ab}^s d$, where d represents the interplanar distance. According to the general London equation Eq. (5), we can get the in-plane superfluid density through $n_{ab}^s = \frac{m^*}{\mu_0 e^2 \lambda_{ab}^2}$.

Correspondingly,

$$T_F = \frac{\pi \hbar^2 \lambda_{ab}^{-2} d}{k_B \mu_0 e^2}, \qquad (11)$$

therefore, T_F of $La_2(Cu_{1-x}Ni_x)_5As_3O_2$ ($x = 0.45$ and 0.40) are estimated, and the results are listed in Table III. As shown in Fig. 4, $La_2(Cu_{1-x}Ni_x)_5As_3O_2$ ($x = 0.40$ and 0.45) fall in the crossover between the unconventional superconducting area and the conventional BCS region. The fact that T_c/T_F is

TABLE III. Uemura plot parameters for $La_2(Cu_{1-x}Ni_x)_5As_3O_2$.

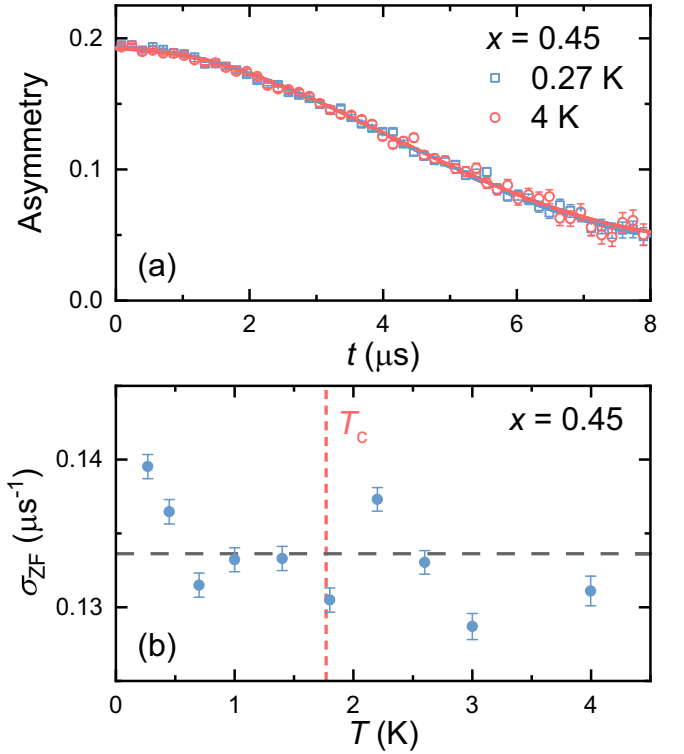| x	$\lambda_{ab}(0)$ (nm)	d (Å)	T_F (K)	T_c (K)	T_c/T_F
0.40	427	22.44	964	2.11	~1/457
0.45	422	22.43	990	1.77	~1/560

FIG. 5. (a) ZF-μSR time spectra at representative temperatures for polycrystalline samples of $La_2(Cu_{1-x}Ni_x)_5As_3O_2$ ($x = 0.45$). Curves: Fits to the data by Eq. (12). The background signal from muons that stops in the copper sample holder has not been subtracted. (b) Temperature dependence of the Gaussian KT relaxation rate σ_{ZF} for $La_2(Cu_{1-x}Ni_x)_5As_3O_2$ ($x = 0.45$). The red dashed line represents T_c determined from the transport measurements. The gray dashed line shows an average of $\sigma_{ZF} = 0.1336$ μs^{-1}.

larger in $x = 0.40$ than 0.45 may suggest a stronger pairing interaction in $x = 0.40$.

C. ZF-μSR

To further investigate the superconductivity in $La_2(Cu_{1-x}Ni_x)_5As_3O_2$, ZF-$\mu$SR experiments were performed. Figure 5(a) shows the time evolution of the decay positron count asymmetry, which is proportional to the muon spin polarization, at temperatures above and below T_c in $x = 0.45$. There is no noticeable difference between the superconducting and the normal state, suggesting the absence of a spontaneous magnetic field below T_c. Therefore, TRS is conserved below the superconducting transition. Over the entire temperature range, the ZF-μSR spectra can be well described by the following function,

$$\frac{A(t)}{A(0)} = (1 - f_{bg}) G_{KT}(t) + f_{bg} G_{bg}(t), \qquad (12)$$

where the two relaxing terms are the signals of the sample and the background. $A(0)$ is the initial total asymmetry at time $t = 0$, and f_{bg} is the proportion of the background signal, which has the same value as the one in the TF-μSR experiments. $G_{KT}(t)$ is the static Gaussian Kubo-Toyabe (KT) function [31]

$$G_{KT}(\sigma_{ZF}, t) = \frac{1}{3} + \frac{2}{3}\left(1 - \sigma_{ZF}^2 t^2\right) \exp\left(-\frac{1}{2}\sigma_{ZF}^2 t^2\right), \qquad (13)$$

where σ_{ZF} is the Gaussian KT relaxation rate which corresponds to the relaxation due to static, randomly oriented local fields associated with the nuclear moments at the muon site. Figure 5(b) shows that there is no significant change in relaxation rate σ_{ZF} down to the base temperature $T = 0.27$ K. The average value of σ_{ZF} is 0.1336 μs^{-1}, consistent with the typical nuclear dipolar moments of Ni and Cu [59–61].

IV. DISCUSSION

Low-temperature investigations are crucial for determining the superconducting pairing mechanism. Our TF-μSR measurements were performed down to 20 mK, and the temperature dependence of superfluid density suggests that the two-band model best fits the data for both measured samples, one of which is dominated by the *s* wave and the other in such a small proportion that we cannot confirm whether it is the *s* wave or the *d* wave under the current data conditions. The two-band superconductivity scenario is also supported by the density functional theory (DFT) calculations showing that two bands crossing the Fermi energy contribute to the Fermi surface in La$_2$Cu$_5$As$_3$O$_2$ [21]. Furthermore, the temperature dependence of the upper critical field $H_{c2}(T)$ of La$_2$(Cu$_{1-x}$Ni$_x$)$_5$As$_3$O$_2$ exhibits an upward curvature [21], significantly different from the Werthamer-Helfand-Hohenberg relation [62], which may also propose multiband superconductivity [63].

BCS superconductivity and Bose-Einstein condensation (BEC) are two asymptotic limits of a fermionic superfluid. Systems with a small $T_c/T_F < 0.001$ are usually considered to be BCS-like, while large T_c/T_F values are expected only in the BEC-like picture and are considered to be a hallmark feature of unconventional superconductivity [40,54,64]. As shown in Fig. 4, La$_2$(Cu$_{1-x}$Ni$_x$)$_5$As$_3$O$_2$ falls in the crossover area between BCS and exotic superconductors regions, as many other superconductors such as TRS breaking superconductors La$_7$Ir$_3$ and LaNiC$_2$ [57,60,65], and multiband iron-based superconductors BaFe$_2$(As$_{1-x}$P$_x$)$_2$ [66]. In the Uemura plot classification scheme, these superconductors may not be traditional electron-phonon coupled BCS superconductors but more as exotic unconventional superconductors.

More experimental evidence is required to investigate whether *d*-wave superconductivity exists in one of the bands. Table II shows that the proportion of the *d* wave decreases as Ni concentration increases if it does exist. Such a behavior is rare but was observed in layered cuprates La$_{2-x}$Ce$_x$CuO$_{4-y}$ and Pr$_{2-x}$Ce$_x$CuO$_{4-y}$, where a transition from *d*- to *s*-

wave pairing occurs near the optimal doping [67]. Also in LaFeAs$_{1-x}$P$_x$O [68], the superconducting order parameter evolves from nodal to nodeless as the doping concentration exceeds 50%. Moreover, a crossover from a nodal to nodeless superconducting energy gap was also suggested in skutterudite PrPt$_4$Ge$_{12}$ through Ce substitution [69,70], although the possibility of a transition from multiband to single-band superconductivity cannot be excluded. In addition, a molecular pairing scenario [45] was proposed to explain the transition from nodal to nodeless superconductivity in Yb-substituted CeCoIn$_5$ [71]. The Yb doping increases the chemical potential and drives a Lifshitz transition of the nodal Fermi surface, forming a fully gapped molecular superfluid of composite pairs. For La$_2$(Cu$_{1-x}$Ni$_x$)$_5$As$_3$O$_2$, the Fermi pocket around the Γ point is relatively small according to the DFT calculations [21], and a detailed electronic structure study is required to investigate whether the molecular pairing scenario can be applied.

V. CONCLUSIONS

In summary, we performed ZF and TF-μSR measurements on the recently discovered layered superconductor La$_2$(Cu$_{1-x}$Ni$_x$)$_5$As$_3$O$_2$ ($x = 0.40$ and 0.45). The preservation of TRS is suggested by the ZF-μSR measurements. In combination with the $H_{c2}(T)$ data and DFT calculations [21], the temperature dependence of the superfluid density of La$_2$(Cu$_{1-x}$Ni$_x$)$_5$As$_3$O$_2$ measured by TF-μSR is best described by the two-band model with the dominant *s*-wave superconducting energy gap larger for optimal doping, suggesting the coupling strength decreases with an increase of doping concentration. Both samples are classified between unusual superconductors and traditional BCS superconductors in the Uemura plot. More experimental evidence is required to investigate whether *d*-wave superconductivity exists in one of the bands.

[1] G. M. Luke, A. Keren, L. P. Le, W. D. Wu, Y. J. Uemura, D. A. Bonn, L. Taillefer, and J. D. Garrett, Muon Spin Relaxation in UPt$_3$, Phys. Rev. Lett. **71**, 1466 (1993).

[2] C. C. Tsuei and J. R. Kirtley, Pairing symmetry in cuprate superconductors, Rev. Mod. Phys. **72**, 969 (2000).

[3] S. A. Kivelson, I. P. Bindloss, E. Fradkin, V. Oganesyan, J. M. Tranquada, A. Kapitulnik, and C. Howald, How to detect fluctuating stripes in the high-temperature superconductors, Rev. Mod. Phys. **75**, 1201 (2003).

[4] A. V. Balatsky, I. Vekhter, and J.-X. Zhu, Impurity-induced states in conventional and unconventional superconductors, Rev. Mod. Phys. **78**, 373 (2006).

[5] S. Onari and H. Kontani, Violation of Anderson's Theorem for the Sign-Reversing *s*-Wave State of Iron-Pnictide Superconductors, Phys. Rev. Lett. **103**, 177001 (2009).

[6] T. Hanaguri, S. Niitaka, K. Kuroki, and H. Takagi, Unconventional *s*-wave superconductivity in Fe(Se,Te), Science **328**, 474 (2010).

[7] T. Wu, H. Mayaffre, S. Krämer, M. Horvatić, C. Berthier, W. N. Hardy, R. Liang, D. A. Bonn, and M.-H. Julien, Magnetic-field-induced charge-stripe order in the high-temperature superconductor YBa$_2$Cu$_3$O$_y$, Nature (London) **477**, 191 (2011).

[8] Z. Guguchia, R. Khasanov, M. Bendele, E. Pomjakushina, K. Conder, A. Shengelaya, and H. Keller, Negative Oxygen Isotope Effect on the Static Spin Stripe Order in Superconducting La$_{2-x}$Ba$_x$CuO$_4$ ($x = 1/8$) Observed by Muon-Spin Rotation, Phys. Rev. Lett. **113**, 057002 (2014).

[9] T. Sarkar, D. S. Wei, J. Zhang, N. R. Poniatowski, P. R. Mandal, A. Kapitulnik, and R. L. Greene, Ferromagnetic order beyond the superconducting dome in a cuprate superconductor, Science **368**, 532 (2020).

[10] I. M. Hayes, D. S. Wei, T. Metz, J. Zhang, Y. S. Eo, S. Ran, S. R. Saha, J. Collini, N. P. Butch, D. F. Agterberg, A. Kapitulnik, and J. Paglione, Multicomponent superconducting order parameter in UTe$_2$, Science **373**, 797 (2021).

[11] B. Nachumi, A. Keren, K. Kojima, M. Larkin, G. M. Luke, J. Merrin, O. Tchernyshöv, Y. J. Uemura, N. Ichikawa, M. Goto, and S. Uchida, Muon Spin Relaxation Studies of Zn-Substitution Effects in High-T_c Cuprate Superconductors, Phys. Rev. Lett. **77**, 5421 (1996).

[12] C. M. Smith, A. H. Castro Neto, and A. V. Balatsky, T_c Suppression in Co-Doped Striped Cuprates, Phys. Rev. Lett. **87**, 177010 (2001).

[13] H. Yang, Z. Wang, D. Fang, Q. Deng, Q. H. Wang, Y. Y. Xiang, Y. Yang, and H. H. Wen, In-gap quasiparticle excitations induced by non-magnetic Cu impurities in Na(Fe$_{0.96}$Co$_{0.03}$Cu$_{0.01}$)As revealed by scanning tunnelling spectroscopy, Nat. Commun. **4**, 2749 (2013).

[14] Z. Guguchia, B. Roessli, R. Khasanov, A. Amato, E. Pomjakushina, K. Conder, Y. J. Uemura, J. M. Tranquada, H. Keller, and A. Shengelaya, Complementary Response of Static Spin-Stripe Order and Superconductivity to Nonmagnetic Impurities in Cuprates, Phys. Rev. Lett. **119**, 087002 (2017).

[15] H. Suhl and B. T. Matthias, Impurity scattering in superconductors, Phys. Rev. **114**, 977 (1959).

[16] P. Anderson, Theory of dirty superconductors, J. Phys. Chem. Solids **11**, 26 (1959).

[17] L. J. Li, Y. K. Luo, Q. B. Wang, H. Chen, Z. Ren, Q. Tao, Y. K. Li, X. Lin, M. He, Z. W. Zhu, G. H. Cao, and Z. A. Xu, Superconductivity induced by Ni doping in BaFe$_2$As$_2$ single crystals, New J. Phys. **11**, 025008 (2009).

[18] G. R. Stewart, Superconductivity in iron compounds, Rev. Mod. Phys. **83**, 1589 (2011).

[19] S. Ideta, T. Yoshida, I. Nishi, A. Fujimori, Y. Kotani, K. Ono, Y. Nakashima, S. Yamaichi, T. Sasagawa, M. Nakajima, K. Kihou, Y. Tomioka, C. H. Lee, A. Iyo, H. Eisaki, T. Ito, S. Uchida, and R. Arita, Dependence of Carrier Doping on the Impurity Potential in Transition-Metal-Substituted FeAs-Based Superconductors, Phys. Rev. Lett. **110**, 107007 (2013).

[20] P. Dai, Antiferromagnetic order and spin dynamics in iron-based superconductors, Rev. Mod. Phys. **87**, 855 (2015).

[21] X. Chen, J. Guo, C. Gong, E. Cheng, C. Le, N. Liu, T. Ying, Q. Zhang, J. Hu, S. Li, and X. Chen, Anomalous dome-like superconductivity in RE$_2$(Cu$_{1-x}$Ni$_x$)$_5$As$_3$O$_2$ (RE = La, Pr, Nd), iScience **14**, 171 (2019).

[22] X. Wu, S. Jiang, F. Pan, J. Lin, N. Xu, Mao Zhiqiang, Xu Gaoji, and Zhang Yuheng, Microstructures of La$_{1.85}$Sr$_{0.15}$CuO$_4$ doped with Ni at high doping level, Phys. C: Supercond. **271**, 331 (1996).

[23] Y. Itoh, S. Adachi, T. Machi, Y. Ohashi, and N. Koshizuka, Ni-substituted sites and the effect on Cu electron spin dynamics of YBa$_2$Cu$_{3-x}$Ni$_x$O$_{7-\delta}$, Phys. Rev. B **66**, 134511 (2002).

[24] A. D. Hillier, S. J. Blundell, I. McKenzie, I. Umegaki, L. Shu, J. A. Wright, T. Prokscha, F. Bert, K. Shimomura, A. Berlie, H. Alberto, and I. Watanabe, Muon spin spectroscopy, Nat. Rev. Methods Primers **2**, 4 (2022).

[25] A. Yaouanc and P. Dalmas de Réotier, *Muon Spin Rotation, Relaxation and Resonance* (Oxford University Press, Oxford, UK, 2011).

[26] J. E. Sonier, W. Huang, C. V. Kaiser, C. Cochrane, V. Pacradouni, S. A. Sabok-Sayr, M. D. Lumsden, B. C. Sales, M. A. McGuire, A. S. Sefat, and D. Mandrus, Magnetism and Disorder Effects on Muon Spin Rotation Measurements of the Magnetic Penetration Depth in Iron-Arsenic Superconductors, Phys. Rev. Lett. **106**, 127002 (2011).

[27] J. Zhang, K. Huang, Z. F. Ding, D. E. MacLaughlin, O. O. Bernal, P.-C. Ho, C. Tan, X. Liu, D. Yazici, M. B. Maple, and L. Shu, Superconducting gap structure in ambient-pressure-grown LaO$_{0.5}$F$_{0.5}$BiS$_2$, Phys. Rev. B **94**, 224502 (2016).

[28] J. Zhang, Z. Ding, C. Tan, K. Huang, O. O. Bernal, P.-C. Ho, G. D. Morris, A. D. Hillier, P. K. Biswas, S. P. Cottrell, H. Xiang, X. Yao, D. E. MacLaughlin, and L. Shu, Discovery of slow magnetic fluctuations and critical slowing down in the pseudogap phase of YBa$_2$Cu$_3$O$_y$, Sci. Adv. **4**, eaao5235 (2018).

[29] C. Tan, T. P. Ying, Z. F. Ding, J. Zhang, D. E. MacLaughlin, O. O. Bernal, P. C. Ho, K. Huang, I. Watanabe, S. Y. Li, and L. Shu, Nodal superconductivity coexists with low-moment static magnetism in single-crystalline tetragonal FeS: A muon spin relaxation and rotation study, Phys. Rev. B **97**, 174524 (2018).

[30] Z. H. Zhu, C. Tan, J. Zhang, P. K. Biswas, A. D. Hillier, M. X. Wang, Y. X. Yang, C. S. Chen, Z. F. Ding, S. Y. Li, and L. Shu, Muon spin rotation and relaxation study on topological noncentrosymmetric superconductor PbTaSe$_2$, New J. Phys. **24**, 023002 (2022).

[31] R. S. Hayano, Y. J. Uemura, J. Imazato, N. Nishida, T. Yamazaki, and R. Kubo, Zero-and low-field spin relaxation studied by positive muons, Phys. Rev. B **20**, 850 (1979).

[32] A. Amato, Heavy-fermion systems studied by μSR technique, Rev. Mod. Phys. **69**, 1119 (1997).

[33] Y. Aoki, A. Tsuchiya, T. Kanayama, S. R. Saha, H. Sugawara, H. Sato, W. Higemoto, A. Koda, K. Ohishi, K. Nishiyama, and R. Kadono, Time-Reversal Symmetry-Breaking Superconductivity in Heavy-Fermion PrOs$_4$Sb$_{12}$ Detected by Muon-Spin Relaxation, Phys. Rev. Lett. **91**, 067003 (2003).

[34] P. Neha, P. K. Biswas, T. Das, and S. Patnaik, Time-reversal symmetry breaking in topological superconductor Sr$_{0.1}$Bi$_2$Se$_3$, Phys. Rev. Mater. **3**, 074201 (2019).

[35] A. Suter and B. Wojek, Musrfit: A free platform-independent framework for μSR data analysis, Phys. Procedia **30**, 69 (2012).

[36] R. Karl, F. Burri, A. Amato, M. Donegà, S. Gvasaliya, H. Luetkens, E. Morenzoni, and R. Khasanov, Muon spin rotation study of type-I superconductivity: Elemental β-Sn, Phys. Rev. B **99**, 184515 (2019).

[37] M. Weber, A. Amato, F. N. Gygax, A. Schenck, H. Maletta, V. N. Duginov, V. G. Grebinnik, A. B. Lazarev, V. G. Olshevsky, V. Y. Pomjakushin, S. N. Shilov, V. A. Zhukov, B. F. Kirillov, A. V. Pirogov, A. N. Ponomarev, V. G. Storchak,

S. Kapusta, and J. Bock, Magnetic-flux distribution and the magnetic penetration depth in superconducting polycrystalline $Bi_2Sr_2Ca_{1-x}Y_xCu_2O_{8+\delta}$ and $Bi_{2-x}Pb_xSr_2CaCu_2O_{8+\delta}$, Phys. Rev. B **48**, 13022 (1993).

[38] A. Maisuradze, R. Khasanov, A. Shengelaya, and H. Keller, Comparison of different methods for analyzing μSR line shapes in the vortex state of type-II superconductors, J. Phys.: Condens. Matter **21**, 075701 (2009).

[39] N. W. Ashcroft and N. D. Mermin, *Solid State Physics* (Saunders College Publishing, Philadelphia, 1976), pp. 657–658.

[40] A. D. Hillier and R. Cywinski, The classification of superconductors using muon spin rotation, Appl. Magn. Reson. **13**, 95 (1997).

[41] Z. F. Ding, J. Zhang, C. Tan, K. Huang, Q. Y. Chen, I. Lum, O. O. Bernal, P.-C. Ho, D. E. MacLaughlin, M. B. Maple, and L. Shu, Renormalizations in unconventional superconducting states of $Ce_{1-x}Yb_xCoIn_5$, Phys. Rev. B **99**, 035136 (2019).

[42] H. Luetkens, H.-H. Klauss, R. Khasanov, A. Amato, R. Klingeler, I. Hellmann, N. Leps, A. Kondrat, C. Hess, A. Köhler, G. Behr, J. Werner, and B. Büchner, Field and Temperature Dependence of the Superfluid Density in $LaFeAsO_{1-x}F_x$ Superconductors: A Muon Spin Relaxation Study, Phys. Rev. Lett. **101**, 097009 (2008).

[43] P. J. Hirschfeld, W. O. Putikka, and D. J. Scalapino, d-wave model for microwave response of high-T_c superconductors, Phys. Rev. B **50**, 10250 (1994).

[44] Y. Wang, M. Li, C. Pei, L. Gao, K. Bu, D. Wang, X. Liu, L. Yan, J. Qu, N. Li, B. Wang, Y. Fang, Y. Qi, and W. Yang, Critical current density and vortex phase diagram in the superconductor $Sn_{0.55}In_{0.45}Te$, Phys. Rev. B **106**, 054506 (2022).

[45] O. Erten, R. Flint, and P. Coleman, Molecular Pairing and Fully Gapped Superconductivity in Yb-Doped $CeCoIn_5$, Phys. Rev. Lett. **114**, 027002 (2015).

[46] E. H. Brandt, Flux distribution and penetration depth measured by muon spin rotation in high-T_c superconductors, Phys. Rev. B **37**, 2349 (1988).

[47] E. H. Brandt, Properties of the ideal Ginzburg-Landau vortex lattice, Phys. Rev. B **68**, 054506 (2003).

[48] W. Barford and J. Gunn, The theory of the measurement of the London penetration depth in uniaxial type II superconductors by muon spin rotation, Phys. C: Supercond. **156**, 515 (1988).

[49] V. Fesenko, V. Gorbunov, and V. Smilga, Analytical properties of muon polarization spectra in type-II superconductors and experimental data interpretation for mono- and polycrystalline HTSCs, Phys. C: Supercond. **176**, 551 (1991).

[50] W. Si, Q. Jie, L. Wu, J. Zhou, G. Gu, P. D. Johnson, and Q. Li, Superconductivity in epitaxial thin films of $Fe_{1.08}Te:O_x$, Phys. Rev. B **81**, 092506 (2010).

[51] H. Padamsee, J. E. Neighbor, and C. A. Shiffman, Quasiparticle phenomenology for thermodynamics of strong-coupling superconductors, J. Low Temp. Phys. **12**, 387 (1973).

[52] A. Carrington and F. Manzano, Magnetic penetration depth of MgB_2, Phys. C: Supercond. **385**, 205 (2003).

[53] R. Khasanov, A. Shengelaya, A. Maisuradze, F. La Mattina, A. Bussmann-Holder, H. Keller, and K. A. Müller, Experimental Evidence for Two Gaps in the High-Temperature $La_{1.83}Sr_{0.17}CuO_4$ Superconductor, Phys. Rev. Lett. **98**, 057007 (2007).

[54] Y. J. Uemura, G. M. Luke, B. J. Sternlieb, J. H. Brewer, J. F. Carolan, W. N. Hardy, R. Kadono, J. R. Kempton, R. F. Kiefl,

S. R. Kreitzman, P. Mulhern, T. M. Riseman, D. L. Williams, B. X. Yang, S. Uchida, H. Takagi, J. Gopalakrishnan, A. W. Sleight, M. A. Subramanian, C. L. Chien *et al.*, Universal Correlations between T_c and $\frac{n_s}{m^*}$ (Carrier Density over Effective Mass) in High-T_c Cuprate Superconductors, Phys. Rev. Lett. **62**, 2317 (1989).

[55] Y. J. Uemura, Condensation, excitation, pairing, and superfluid density in high-T_c superconductors: the magnetic resonance mode as a roton analogue and a possible spin-mediated pairing, J. Phys.: Condens. Matter **16**, S4515 (2004).

[56] Y. Nakagawa, Y. Kasahara, T. Nomoto, R. Arita, T. Nojima, and Y. Iwasa, Gate-controlled BCS-BEC crossover in a two-dimensional superconductor, Science **372**, 190 (2021).

[57] J. A. T. Barker, B. D. Breen, R. Hanson, A. D. Hillier, M. R. Lees, G. Balakrishnan, D. M. Paul, and R. P. Singh, Superconducting and normal-state properties of the noncentrosymmetric superconductor Re_3Ta, Phys. Rev. B **98**, 104506 (2018).

[58] L. Benfatto, S. Caprara, C. Castellani, A. Paramekanti, and M. Randeria, Phase fluctuations, dissipation, and superfluid stiffness in d-wave superconductors, Phys. Rev. B **63**, 174513 (2001).

[59] G. M. Luke, J. H. Brewer, S. R. Kreitzman, D. R. Noakes, M. Celio, R. Kadono, and E. J. Ansaldo, Muon diffusion and spin dynamics in copper, Phys. Rev. B **43**, 3284 (1991).

[60] A. D. Hillier, J. Quintanilla, and R. Cywinski, Evidence for Time-Reversal Symmetry Breaking in the Noncentrosymmetric Superconductor $LaNiC_2$, Phys. Rev. Lett. **102**, 117007 (2009).

[61] S. K. P., D. Singh, A. D. Hillier, and R. P. Singh, Probing nodeless superconductivity in LaMSi ($M =$ Ni, Pt) using muon-spin rotation and relaxation, Phys. Rev. B **102**, 094515 (2020).

[62] N. R. Werthamer, E. Helfand, and P. C. Hohenberg, Temperature and purity dependence of the superconducting critical field, H_{c2}. III. Electron spin and spin-orbit effects, Phys. Rev. **147**, 295 (1966).

[63] F. Hunte, J. Jaroszynski, A. Gurevich, D. C. Larbalestier, R. Jin, A. S. Sefat, M. A. McGuire, B. C. Sales, D. K. Christen, and D. Mandrus, Two-band superconductivity in $LaFeAsO_{0.89}F_{0.11}$ at very high magnetic fields, Nature (London) **453**, 903 (2008).

[64] Y. J. Uemura, L. P. Le, G. M. Luke, B. J. Sternlieb, W. D. Wu, J. H. Brewer, T. M. Riseman, C. L. Seaman, M. B. Maple, M. Ishikawa, D. G. Hinks, J. D. Jorgensen, G. Saito, and H. Yamochi, Basic Similarities Among Cuprate, Bismuthate, Organic, Chevrel-Phase, and Heavy-Fermion Superconductors Shown by Penetration-Depth Measurements, Phys. Rev. Lett. **66**, 2665 (1991).

[65] J. A. T. Barker, D. Singh, A. Thamizhavel, A. D. Hillier, M. R. Lees, G. Balakrishnan, D. M. Paul, and R. P. Singh, Unconventional Superconductivity in La_7Ir_3 Revealed by Muon Spin Relaxation: Introducing a New Family of Noncentrosymmetric Superconductor That Breaks Time-Reversal Symmetry, Phys. Rev. Lett. **115**, 267001 (2015).

[66] K. Hashimoto, K. Cho, T. Shibauchi, S. Kasahara, Y. Mizukami, R. Katsumata, Y. Tsuruhara, T. Terashima, H. Ikeda, M. A. Tanatar, H. Kitano, N. Salovich, R. W. Giannetta, P. Walmsley, A. Carrington, R. Prozorov, and Y. Matsuda, A sharp peak of the zero-temperature penetration depth at optimal composition in $BaFe_2(As_{1-x}P_x)_2$, Science **336**, 1554 (2012).

[67] J. A. Skinta, M.-S. Kim, T. R. Lemberger, T. Greibe, and M. Naito, Evidence for a Transition in the Pairing

Symmetry of the Electron-Doped Cuprates $La_{2-x}Ce_xCuO_{4-y}$ and $Pr_{2-x}Ce_xCuO_{4-y}$, Phys. Rev. Lett. **88**, 207005 (2002).

[68] T. Shiroka, N. Barbero, R. Khasanov, N. D. Zhigadlo, H. R. Ott, and J. Mesot, Nodal-to-nodeless superconducting order parameter in $LaFeAs_{1-x}P_xO$ synthesized under high pressure, npj Quantum Mater. **3**, 25 (2018).

[69] A. Maisuradze, M. Nicklas, R. Gumeniuk, C. Baines, W. Schnelle, H. Rosner, A. Leithe-Jasper, Y. Grin, and R. Khasanov, Superfluid Density and Energy Gap Function of Superconducting $PrPt_4Ge_{12}$, Phys. Rev. Lett. **103**, 147002 (2009).

[70] K. Huang, L. Shu, I. K. Lum, B. D. White, M. Janoschek, D. Yazici, J. J. Hamlin, D. A. Zocco, P.-C. Ho, R. E. Baumbach, and M. B. Maple, Probing the superconductivity of $PrPt_4Ge_{12}$ through Ce substitution, Phys. Rev. B **89**, 035145 (2014).

[71] H. Kim, M. A. Tanatar, R. Flint, C. Petrovic, R. Hu, B. D. White, I. K. Lum, M. B. Maple, and R. Prozorov, Nodal to Nodeless Superconducting Energy-Gap Structure Change Concomitant with Fermi-Surface Reconstruction in the Heavy-Fermion Compound $CeCoIn_5$, Phys. Rev. Lett. **114**, 027003 (2015).